LETTERS

Myosin II contributes to cell-scale actin network treadmilling through network disassembly

Cyrus A. Wilson[1]†, Mark A. Tsuchida[1], Greg M. Allen[1], Erin L. Barnhart[1], Kathryn T. Applegate[2], Patricia T. Yam[1]†, Lin Ji[2], Kinneret Keren[1]†, Gaudenz Danuser[2]† & Julie A. Theriot[1,3]

Crawling locomotion of eukaryotic cells is achieved by a process dependent on the actin cytoskeleton[1]: protrusion of the leading edge requires assembly of a network of actin filaments[2], which must be disassembled at the cell rear for sustained motility. Although ADF/cofilin proteins have been shown to contribute to actin disassembly[3], it is not clear how activity of these locally acting proteins could be coordinated over the distance scale of the whole cell. Here we show that non-muscle myosin II has a direct role in actin network disassembly in crawling cells. In fish keratocytes undergoing motility, myosin II is concentrated in regions at the rear with high rates of network disassembly. Activation of myosin II by ATP in detergent-extracted cytoskeletons results in rear-localized disassembly of the actin network. Inhibition of myosin II activity and stabilization of actin filaments synergistically impede cell motility, suggesting the existence of two disassembly pathways, one of which requires myosin II activity. Our results establish the importance of myosin II as an enzyme for actin network disassembly; we propose that gradual formation and reorganization of an actomyosin network provides an intrinsic destruction timer, enabling long-range coordination of actin network treadmilling in motile cells.

A thorough understanding of actin polymerization-based crawling at the whole-cell scale has long been a challenge in the field of cell biology. A combination of biochemical and cell-biological experiments has led to a consensus model for the mechanism by which steady-state actin network treadmilling in the lamellipodia of motile cells contributes to protrusion of the leading edge: new filaments are nucleated near the leading edge, resulting in the assembly of a branched actin network, which is eventually disassembled by ADF/cofilin proteins, replenishing the pool of polymerizable actin monomers[3].

However, extending this model from the micrometre scale of the leading edge lamellipodium to the tens-of-micrometres scale of an entire cell requires a mechanism for longer-range coordination: a cell-scale spatial organization of network assembly and disassembly processes, giving rise to sustained whole-cell motility. The molecular mechanisms of actin network disassembly and its spatial regulation in motile cells are not completely understood (Supplementary Information).

Here we use fish epidermal keratocytes (Fig. 1a) as a model system to investigate the spatial regulation of actin network turnover in motile cells. These cells are fast-moving with persistent velocity and shape[4] and maintain a continuous actin network throughout the lamellipodium[5,6] (Fig. 1b), implying that the net rates of assembly at the front and disassembly at the rear must be closely and constantly coordinated. This property allows us to analyse network turnover based on steady-state measurements.

To investigate the spatial organization of actin network movement and dynamics, we performed fluorescence speckle microscopy (FSM) on cells moving at steady state (Fig. 1b). The direction and speed of actin network movement was determined by speckle flow tracking[7] as a function of position within the lamellipodium (Fig. 1c). Consistent with photoactivation experiments[2], we found that the actin network in the lamellipodium remains nearly stationary with respect to the substrate, with minimal retrograde flow (Fig. 1c). At the cell rear, the actin network moved forward and rapidly inward from the sides.

To analyse the movement of the actin network relative to the boundaries of these fast-moving cells, we represented the FSM flow field in the cell's moving frame of reference[8] (Fig. 1d and Supplementary Movie 1). In the cell frame of reference, movement of the network appeared uniform and rearward in the front of the cell, and almost completely perpendicular to the direction of motion at the

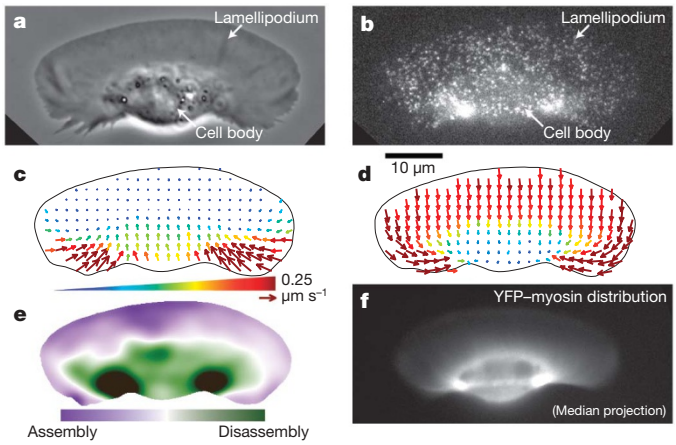

Figure 1 | Myosin II in keratocytes co-localizes with the primary sites of actin network disassembly. **a**–**e**, Data and analysis of a single live keratocyte. **a**, Phase-contrast image of the keratocyte moving upwards. **b**, FSM image of the actin network labelled with a low concentration of phalloidin. **c**, F-actin flow field based on speckle tracking, in the laboratory frame of reference. Arrow length and colour both indicate the speed of actin network flow. **d**, F-actin flow field in the cell frame of reference. **e**, Steady-state net F-actin assembly and disassembly. **f**, Fluorescence image of YFP-tagged myosin regulatory light chain in a keratocyte of similar size and shape to that shown in **a**–**e**. Myosin II is found at low levels throughout the lamellipodium and at the highest concentrations in two foci flanking the cell body, which coincide with the primary sites of actin network disassembly as shown in **e**.

[1]Department of Biochemistry and Howard Hughes Medical Institute, Stanford University School of Medicine, Stanford, California 94305, USA. [2]Department of Cell Biology, The Scripps Research Institute, La Jolla, California 92037, USA. [3]Department of Microbiology and Immunology, Stanford University School of Medicine, Stanford, California 94305, USA. †Present addresses: Institute for Creative Technologies, University of Southern California, Marina del Rey, California 90292, USA (C.A.W.); Montreal Neurological Institute, Montreal, Quebec, H3A 2B4, Canada (P.T.Y.); Department of Physics and the Russell Berrie Nanotechnology Institute, Technion – Israel Institute of Technology, Haifa 32000, Israel (K.K.); Department of Cell Biology, Harvard Medical School, Boston, Massachusetts 02115, USA (G.D.).

rear sides. Under the cell body, network flow ceased without significantly changing its direction.

The pattern of fluorescent speckle motion suggests that net actin network assembly occurred in the front of the cell and net disassembly in the rear. This was confirmed by calculating the spatial distribution of net filamentous actin (F-actin) assembly and disassembly, using actin speckle density and the divergence of the FSM flow field[9] (Fig. 1e and Supplementary Fig. 2a). Intriguingly, we found that the rear-localized pattern of disassembly, with two foci flanking the cell body, was strongly reminiscent of the distribution of myosin II, as visualized by yellow fluorescent protein (YFP)-tagged myosin II regulatory light chain (Fig. 1f).

Although the role of myosin II in the rear of motile cells is conventionally associated with mechanical force generation and contraction (Supplementary Information), several lines of evidence raise the possibility that myosin II may also have a specific role in driving actin network disassembly. Spatially correlated contraction and actin depolymerization in motile cells has been shown to be promoted by a drug that stimulates myosin II activity[9]. In cytokinesis, where contraction of the cleavage furrow is driven in part by myosin II motor activity, inhibition of myosin II leads to increased accumulation of F-actin in the cleavage furrow, consistent with a role for myosin II in regulating or catalysing F-actin disassembly in the contractile ring[10,11]. During the early steps of inner-ear morphogenesis, myosin II activity is required for depletion of F-actin from the basal cortex of an ectodermal sheet[12]. More directly, myosin II has been shown to potentiate severing and disassembly of actin filament bundles at the base of neuronal growth cones[13]. Finally, in a recent *in vitro* experiment, a loss of actin filaments in solution was observed in the presence of purified myosin II[14].

Our observation of disassembly co-localized with myosin II density suggested that such a link between myosin II activity and actin network disassembly might be at work in keratocyte motility. To investigate this possibility, we treated keratocytes with the myosin II ATPase inhibitor blebbistatin[15]. Although blebbistatin-treated cells continued to move with little shape change at the leading edge (Fig. 2 and Supplementary Movie 1) and with only a moderate decrease in speed (Fig. 3f), the pattern of disassembly was markedly altered: the two foci of disassembly adjacent to the cell body disappeared, and disassembly was distributed along the trailing edge (Fig. 2e and Supplementary Information).

Continued motility of keratocytes under blebbistatin treatment indicates that at least some disassembly activity of the actin network was retained. We judged that inhibition of myosin II was essentially complete under the conditions of our blebbistatin treatment (50 μM active enantiomer, 10 min) based on two criteria. First, two aspects of motility that are normally attributed to myosin II activity (Supplementary Information) were reduced below the detection limit: inward flow in the cell rear (Fig. 2b–d and Supplementary Movie 1) and inward traction force (Supplementary Fig. 3 and Supplementary Movie 2). Second, increasing the blebbistatin concentration by two-fold did not have a further effect on cell speed (data not shown). These observations led us to hypothesize that there may be a parallel pathway that disassembles the actin network independent of myosin II.

We thus proceeded to examine the effect of myosin II inhibition in a sensitized background where actin depolymerization was partly inhibited. The F-actin stabilizing drug jasplakinolide[11,16], at 1 μM, decreased cell speed moderately, an effect comparable to that of 50 μM blebbistatin (Fig. 3f). For cells pre-incubated with 50 μM blebbistatin, however, 1 μM jasplakinolide dramatically inhibited motility (Fig. 3a, b, f and Supplementary Movie 3), often causing a rapid and complete cessation of both movement and actin network flow (Fig. 3a, b and Supplementary Movie 3). To test the specificity of this synthetic effect, we examined the effect of latrunculin A, which slows actin network turnover by sequestering monomer (inhibiting polymerization) rather than by inhibiting depolymerization. Although 50 nM latrunculin A caused keratocytes to lose polarity

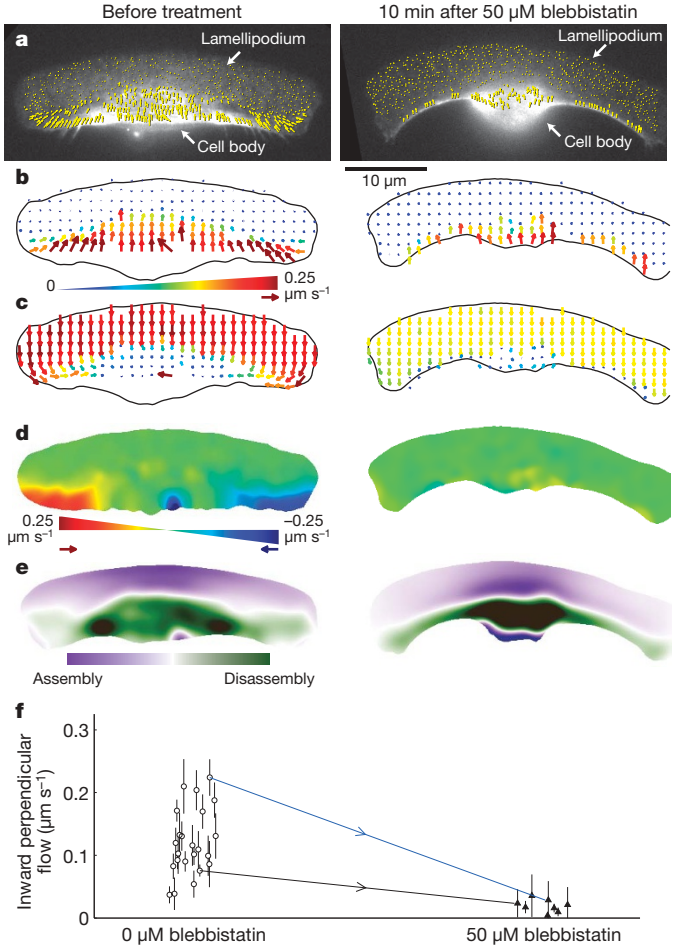

Figure 2 | Inhibition of myosin II blocks inward flow and alters the pattern of disassembly of the actin network. **a**–**e**, Analysis of actin network flow in a single keratocyte before (left) and approximately 10 min after (right) addition of 50 μM blebbistatin. **a**, Raw F-actin speckle flow measurements (yellow arrows) in the laboratory frame of reference, superimposed on the corresponding FSM frames. **b**, Resampled flow field in the laboratory frame of reference. **c**, Resampled flow field in the cell frame of reference. **d**, Maps showing the component of network flow perpendicular to the direction of cell movement ('perpendicular flow') in the cell frame of reference. Red indicates F-actin flow towards the right; blue, towards the left. Actin network movement in the green regions is parallel to the direction of cell locomotion. Blebbistatin treatment abolishes inward flow. **e**, Steady-state assembly/disassembly maps. Before blebbistatin treatment, the highest rate of disassembly is found in two foci flanking the cell body. After blebbistatin treatment, disassembly is distributed along the rear margin. **f**, Inward perpendicular flow of the actin network in untreated (white circles; $n = 23$) and blebbistatin-treated (black triangles; $n = 8$) cells. Error bars indicate average ± s.d. over each movie (typically 4 min). Measurements were made before and after treatment for two of the cells; blue and black arrows connect the corresponding data points. The data points connected by the blue arrow correspond to the cell shown in **a**–**e**. Compare with Supplementary Movie 1.

and stop moving (data not shown), 5 nM latrunculin A caused a speed decrease comparable to sole treatment with either 50 μM blebbistatin or 1 μM jasplakinolide (Fig. 3f). Treatment with the combination of blebbistatin and latrunculin A, or jasplakinolide and latrunculin A, did not have a synthetic effect on cell speed (Fig. 3f). This suggested that the synthetic effect was not simply a result of actin monomer depletion, but specific to disassembly inhibition. Both blebbistatin-treated cells and jasplakinolide-treated cells showed an unusual accumulation of F-actin in the cell rear, but the patterns were distinct: in blebbistatin-treated cells, F-actin accumulated primarily along the trailing edge and in tail-like structures (Fig. 3d, g), whereas in jasplakinolide-treated cells F-actin accumulated under the cell body (Fig. 3e, g). These observations are consistent with the existence of

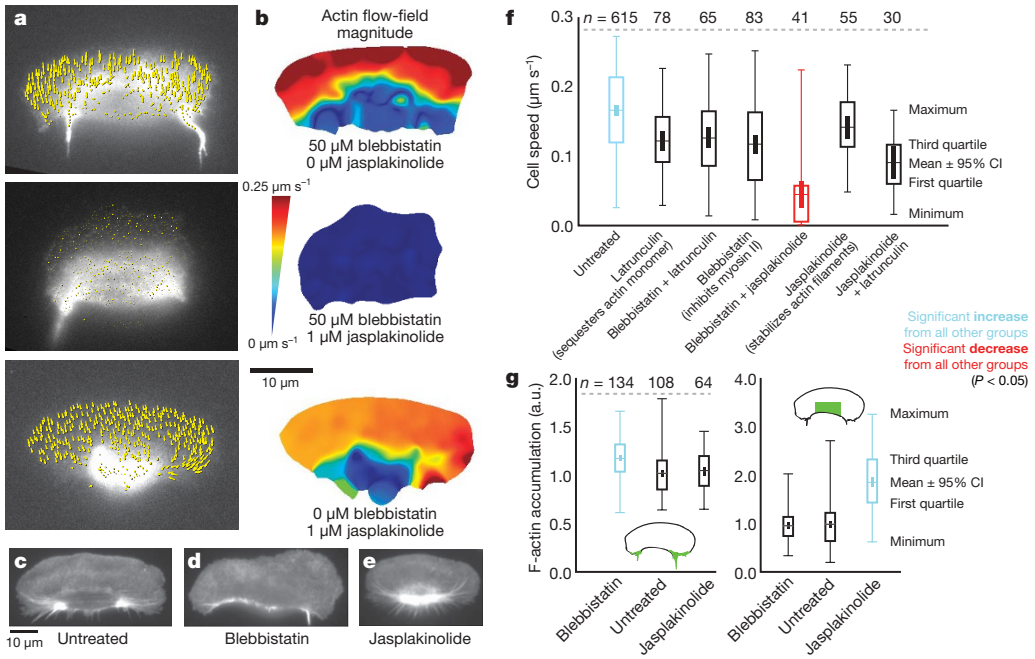

Figure 3 | Jasplakinolide specifically halts actin dynamics of cells in which myosin II is inhibited. **a**, Raw F-actin speckle flow measurements in the cell frame of reference (yellow arrows) superimposed on the corresponding FSM frames, for a cell in 50 μM blebbistatin before (top) and approximately 2 min after (middle) addition of 1 μM jasplakinolide. Bottom, a separate cell in jasplakinolide alone. **b**, F-actin flow magnitude maps corresponding to **a**. The combination of blebbistatin and jasplakinolide immobilizes the actin network, an effect that is not achieved by either drug alone. **c**–**e**, Fixed, phalloidin-labelled keratocytes, untreated (**c**) or treated with 50 μM blebbistatin (**d**) or 1 μM jasplakinolide (**e**). Consistent with impaired actin-network disassembly, blebbistatin-treated cells accumulate F-actin along the rear margin, jasplakinolide-treated cells underneath the cell body. **f**, Treatment with either 5 nM latrunculin A, 50 μM blebbistatin or 1 μM jasplakinolide can slow cells relative to the control population. The combination of blebbistatin and latrunculin A or jasplakinolide and latrunculin A has no significant further effect on cell speed than either drug alone. The combination of blebbistatin and jasplakinolide significantly ($P < 0.05$ by Tukey's test) and synergistically slows cell locomotion. **g**, Blebbistatin causes significant ($P < 0.05$ by Tukey's test) F-actin accumulation in the trailing 'tails' (but not in the cell body), whereas jasplakinolide causes accumulation underneath the cell body (but not in the 'tails'), relative to untreated cells. a.u., Arbitrary units (see Methods). Compare **c**–**e**. Box-and-whisker plots (**f** and **g**) indicate the mean, 95% confidence interval (CI), extrema and quartiles for the indicated number of cells (n) in each treatment group. Compare with Supplementary Movie 3.

two complementary and partly redundant mechanisms for actin network disassembly: one dependent on myosin II activity, the other inhibited by jasplakinolide.

Our *in vivo* experiments do not distinguish between a direct or indirect contribution of myosin II activity to actin network disassembly. To investigate the specific contribution of myosin II activity, it was essential to analyse disassembly of the rear network in isolation—in the absence of the continuous replenishment that occurs in a live forward-moving cell—and to exclude the action of cytosolic factors. Accordingly, we performed experiments using isolated cytoskeletons of Triton X-100-extracted keratocytes[6]. Strikingly, addition of ATP to the extracted cytoskeletons caused not only a rapid inward contraction at the cell rear but also a concomitant dissolution of the actin network in that region (Fig. 4a–d, Supplementary Movie 4 and Supplementary Fig. 6). The leading edge of the cell was not significantly affected by this process. The rear-dominant disassembly of actin (as well as contraction) was significantly suppressed (sometimes to undetectable levels) when cells were incubated with blebbistatin before the detergent extraction (Fig. 4e–h, Supplementary Movie 4 and Supplementary Fig. 6). The ATP dependence, blebbistatin sensitivity, rear localization and synchrony with contraction of the network disassembly are consistent with myosin II as the active agent, and recapitulation of this myosin-II-dependent disassembly in extracted cells strongly suggests that soluble proteins are not required for this process.

To test for the possibility that an unrelated mechanism was protecting the actin network in the front of the cell from disassembly, we treated extracted cytoskeletons with the gelsolin-family Ca^{2+}-dependent actin severing protein villin[17,18], in the absence of ATP. Glutathione *S*-transferase (GST)–villin solubilized F-actin in most regions of the cell, including the front (Fig. 4i–l and Supplementary Movie 4). Interestingly, however, a portion of the network in the rear was relatively insensitive to GST–villin. This region of the network, which lingered during prolonged villin treatment (Supplementary Movie 4), was reminiscent of the pattern of myosin II localization (Fig. 1f) and net actin network disassembly in intact cells (Fig. 1e) and complementary to the pattern of actin network stability after ATP treatment. Addition of both ATP and GST–villin, in either order, gave nearly complete destruction of the actin cytoskeleton (Fig. 4m–t and Supplementary Movie 4). Thus the rear-dominant pattern of ATP-dependent disassembly (Fig. 4a–d) is not due to other regions being impervious to disassembly per se; it probably reflects regions where myosin II is abundant and integrated into the actin network in a configuration that brings about maximal disassembling activity.

Our combined experimental observations point to a direct role for myosin II in actin network disassembly in motile keratocytes of fish. A second, unidentified disassembly mechanism appears to act in parallel with myosin II in unperturbed cells. We found this pathway to be sensitive to jasplakinolide, and we conjecture that it may involve cofilin or gelsolin activity (Supplementary Information). Previous reports showing that F-actin disassembly increases upon stimulation of myosin II phosphorylation[9] and that jasplakinolide selectively halts actin turnover in regions of cells lacking myosin II[19] are consistent with these conclusions.

The observed spatial and temporal coincidence of contraction and disassembly (Figs 1 and 4; ref. 9) is most consistent with a simple mechanism for network disassembly by myosin II: mechanical breakage of actin filaments[20]. Such an effect could be assisted by the ability of the non-muscle myosin II motor domain to bind actin filaments stably when under tension[21], and may represent a common feature of

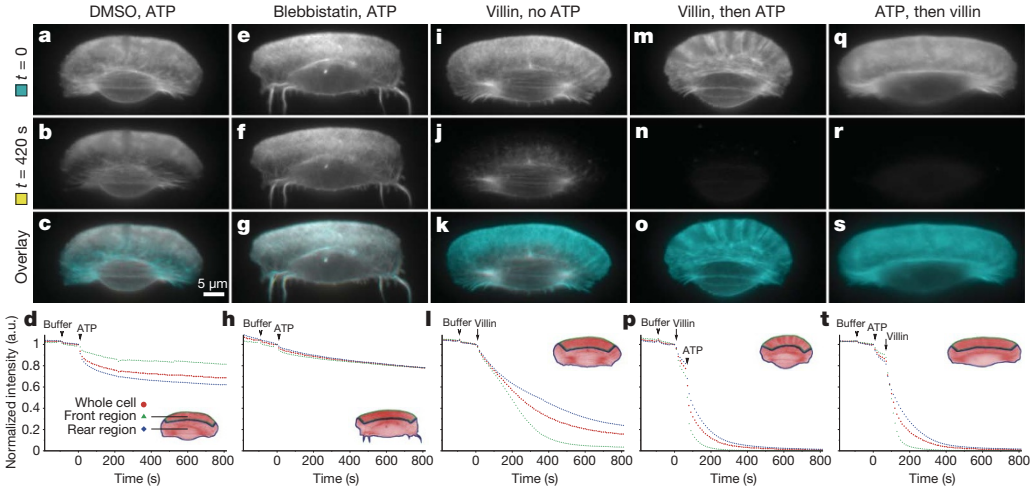

Figure 4 | Actin network disassembly in the rear of detergent-extracted keratocyte cytoskeletons is ATP dependent and blebbistatin sensitive, consistent with a direct role for myosin II in this process. a–d, ATP triggers an acute loss of actin network in the rear region of the cell, where myosin II is localized (compare with Fig. 1f). **a**, A detergent-extracted and phalloidin-labelled keratocyte cytoskeleton[6]. **b**, The same cytoskeleton 7 min after addition of 1 mM ATP. **c**, Overlay of initial frame (**a**, cyan) and frame at 7 min (**b**, yellow); regions with increase, decrease or no change in net intensity appear yellow, cyan or white, respectively. **d**, Time evolution of fluorescence intensities (normalized at $t = 0$) in the indicated regions. Time points for a mock buffer wash (chevron) and ATP addition (black arrowhead) are indicated. **e–h**, In a cell treated with 50 μM blebbistatin for 30 min before extraction, addition of ATP does not induce a loss of actin network. There is a slow loss of fluorescence owing to photobleaching or background dissociation. **i–l**, The F-actin severing protein villin rapidly disassembles the lamellipodial actin network, demonstrating that this part of the cytoskeleton is not protected against a general disassembling activity. GST–villin (0.1 μM) was added instead of ATP (arrow in **l**). **m–t**, Addition of GST–villin (arrows in **p**, **t**) in addition to ATP (arrowheads in **p**, **t**), in either order, results in complete, rapid disassembly of the actin network. Compare with Supplementary Movie 4.

myosin II function in all but the most specialized organization found in striated muscle.

The contribution of myosin-II-driven network disassembly to whole-cell motility may vary in different cell types, depending on the spatial arrangement of the cytoskeletal elements. In keratocytes, we find myosin II to be concentrated at the cell rear and to contribute to cell-scale network treadmilling; given the similar localization of myosin II to the rear in *Dictyostelium*[22] and neutrophils[23], we suggest that its role there may be very similar. In contrast, myosin II in neurons appears to be involved in network disassembly at the base of growth cones[13]. In fibroblasts and larger epithelial cells, the concentration of myosin II in the lamella (behind the lamellipodium) may primarily contribute to local network disassembly in the transition zone between the lamellipodial and lamellar networks[19,24].

The involvement of myosin II in actin network disassembly motivates an appealing model for the long-range spatial and temporal coordination of disassembly in motile cells (Supplementary Fig. 1): slow incorporation of myosin II into the network and subsequent myosin-II-mediated rearrangement of F-actin occur over the same time scale as whole cell translocation[6], serving as a timing mechanism. Progressively assembled myosin II bipolar filaments gradually coalesce the initially dendritic actin network into a more parallel organization[6] that allows efficient action of the myosin II motor, eventually leading to disassembly. The spatiotemporal organization of myosin II incorporation and actin network rearrangement takes place at a large enough scale to serve as a basis for cell-scale treadmilling of the actin cytoskeleton during steady-state motility in these cells.

METHODS SUMMARY

Keratocytes from the Central American cichlid *Hypsophrys nicaraguensis* were prepared for FSM by introducting Alexa Fluor 546 phalloidin by small-volume electroporation as described[25]. We acquired phase-contrast and epifluorescence images through a ×60 (numerical aperture 1.4) objective at 2-s time intervals unless otherwise noted. Using phase-contrast images, we tracked whole-cell movement and calculated transformations between the laboratory and cell frames of reference, as described[8]. We performed F-actin flow tracking on fluorescence images in the cell frame of reference using the adaptive multi-frame correlation algorithm described in ref. 7. For comparisons between cells and over time, velocity fields were binned into five subcellular regions. Time-averaged velocity fields (v) and F-actin signal (ρ) were used to calculate steady-state maps of net F-actin turnover by calculating $\nabla\cdot(\rho v)$ (similar to ref. 9).

Pharmacological treatments were performed while imaging, to capture changes as drugs took effect, by changing the buffer to one containing a new drug or drug combination. We inhibited myosin II with 100 μM (±)-blebbistatin or 50 μM (−)-blebbistatin (the active enantiomer, whose concentration is indicated in the text, figures and movies). To examine the effects on F-actin distribution, we treated keratocytes with blebbistatin or jasplakinolide, fixed them with 4% formaldehyde, permeabilized with 0.5% Triton X-100, and labelled with TRITC-phalloidin. Myosin II localization was visualized by transfection[26] with YFP-tagged *Xenopus laevis* myosin II regulatory light chain[25].

Detergent-extracted cytoskeletons were obtained by the method of Svitkina *et al.*[6] and labelled with TRITC-phalloidin. The acute changes upon addition of 1 mM ATP or 0.1 μM GST–villin were observed by epifluorescence imaging at a 10-s time interval. An ATP-regenerating system was used to preclude inhibition of myosin II by accumulated ADP.

Full Methods and any associated references are available in the online version of the paper at www.nature.com/nature.

Received 22 June 2007; accepted 4 March 2010.

1. Abercrombie, M. The Croonian lecture, 1978: the crawling movement of metazoan cells. *Proc. R. Soc. Lond. B* **207,** 129–147 (1980).
2. Theriot, J. A. & Mitchison, T. J. Actin microfilament dynamics in locomoting cells. *Nature* **352,** 126–131 (1991).
3. Pollard, T. D. & Borisy, G. G. Cellular motility driven by assembly and disassembly of actin filaments. *Cell* **112,** 453–465 (2003).
4. Euteneuer, U. & Schliwa, M. Persistent, directional motility of cells and cytoplasmic fragments in the absence of microtubules. *Nature* **310,** 58–61 (1984).
5. Small, J. V., Herzog, M., Häner, M. & Abei, U. Visualization of actin filaments in keratocyte lamellipodia: negative staining compared with freeze-drying. *J. Struct. Biol.* **113,** 135–141 (1994).
6. Svitkina, T. M., Verkhovsky, A. B., McQuade, K. M. & Borisy, G. G. Analysis of the actin-myosin II system in fish epidermal keratocytes: mechanism of cell body translocation. *J. Cell Biol.* **139,** 397–415 (1997).
7. Ji, L. & Danuser, G. Tracking quasi-stationary flow of weak fluorescent signals by adaptive multi-frame correlation. *J. Microsc.* **220,** 150–167 (2005).
8. Wilson, C. A. & Theriot, J. A. A correlation-based approach to calculate rotation and translation of moving cells. *IEEE Trans. Image Process.* **15,** 1939–1951 (2006).
9. Vallotton, P., Gupton, S. L., Waterman-Storer, C. M. & Danuser, G. Simultaneous mapping of filamentous actin flow and turnover in migrating cells by quantitative

fluorescent speckle microscopy. *Proc. Natl Acad. Sci. USA* **101,** 9660–9665 (2004).
10. Guha, M., Zhou, M. & Wang, Y.-L. Cortical actin turnover during cytokinesis requires myosin II. *Curr. Biol.* **15,** 732–736 (2005).
11. Murthy, K. & Wadsworth, P. Myosin-II-dependent localization and dynamics of F-actin during cytokinesis. *Curr. Biol.* **15,** 724–731 (2005).
12. Sai, X. & Ladher, R. K. FGF signaling regulates cytoskeletal remodeling during epithelial morphogenesis. *Curr. Biol.* **18,** 976–981 (2008).
13. Medeiros, N. A., Burnette, D. T. & Forscher, P. Myosin II functions in actin-bundle turnover in neuronal growth cones. *Nature Cell Biol.* **8,** 215–226 (2006).
14. Haviv, L., Gillo, D., Backouche, F. & Bernheim-Groswasser, A. A cytoskeletal demolition worker: myosin II acts as an actin depolymerization agent. *J. Mol. Biol.* **375,** 325–330 (2008).
15. Straight, A. F. *et al.* Dissecting temporal and spatial control of cytokinesis with a myosin II inhibitor. *Science* **299,** 1743–1747 (2003).
16. Bubb, M. R., Senderowicz, A. M., Sausville, E. A., Duncan, K. L. & Korn, E. D. Jasplakinolide, a cytotoxic natural product, induces actin polymerization and competitively inhibits the binding of phalloidin to F-actin. *J. Biol. Chem.* **269,** 14869–14871 (1994).
17. Bretscher, A. & Weber, K. Villin is a major protein of the microvillus cytoskeleton which binds both G and F actin in a calcium-dependent manner. *Cell* **20,** 839–847 (1980).
18. Glenney, J. R. Jr, Kaulfus, P. & Weber, K. F actin assembly modulated by villin: Ca^{++}-dependent nucleation and capping of the barbed end. *Cell* **24,** 471–480 (1981).
19. Ponti, A., Machacek, M., Gupton, S. L., Waterman-Storer, C. M. & Danuser, G. Two distinct actin networks drive the protrusion of migrating cells. *Science* **305,** 1782–1786 (2004).
20. Kron, S. J. & Spudich, J. A. Fluorescent actin filaments move on myosin fixed to a glass surface. *Proc. Natl Acad. Sci. USA* **83,** 6272–6276 (1986).
21. Kovács, M., Thirumurugan, K., Knight, P. J. & Sellers, J. R. Load-dependent mechanism of nonmuscle myosin 2. *Proc. Natl Acad. Sci. USA* **104,** 9994–9999 (2007).
22. Yumura, S., Mori, H. & Fukui, Y. Localization of actin and myosin for the study of ameboid movement in *Dictyostelium* using improved immunofluorescence. *J. Cell Biol.* **99,** 894–899 (1984).
23. Keller, H. U. & Niggli, V. Colchicine-induced stimulation of PMN motility related to cytoskeletal changes in actin, α-actinin, and myosin. *Cell Motil. Cytoskeleton* **25,** 10–18 (1993).
24. Vicente-Manzanares, M., Zareno, J., Whitmore, L., Choi, C. K. & Horwitz, A. F. Regulation of protrusion, adhesion dynamics, and polarity by myosins IIA and IIB in migrating cells. *J. Cell Biol.* **176,** 573–580 (2007).
25. Yam, P. T. *et al.* Actin–myosin network reorganization breaks symmetry at the cell rear to spontaneously initiate polarized cell motility. *J. Cell Biol.* **178,** 1207–1221 (2007).
26. Lacayo, C. I. *et al.* Emergence of large-scale cell morphology and movement from local actin filament growth dynamics. *PLoS Biol.* **5,** e233 (2007).

Supplementary Information is linked to the online version of the paper at www.nature.com/nature.

Acknowledgements We thank M. J. Footer for the gift of purified GST–villin, A. Mogilner and S. Sivaramakrishnan for discussions, and Z. Pincus, N. Dye and T. Y.-C. Tsai for reading the manuscript. C.A.W. and J.A.T. were supported by National Institutes of Health grant R01AI067712 (J.A.T.). M.A.T. and E.L.B. were supported by National Institutes of Health grant T32GM007276. G.M.A. was supported by the Stanford Medical Scientist Training Program. P.T.Y. was supported by a Howard Hughes Medical Institute Predoctoral Fellowship, Stanford Graduate Fellowship and a Skye International Foundation Scholarship. K.T.A. was supported by a National Science Foundation Graduate Research Fellowship. K.K. was a Damon Runyon Fellow supported by the Damon Runyon Cancer Research Foundation (DRG-#1854-05). K.T.A., L.J. and G.D. were supported by National Institutes of Health grants U54GM64346 and U01GM67230 (G.D.). J.A.T. was supported by the Howard Hughes Medical Institute.

Author Contributions C.A.W., M.A.T. and J.A.T. conceived and designed the experiments. C.A.W. and P.T.Y. performed FSM on untreated motile keratocytes. C.A.W. performed the pharmacological manipulation experiments, FSM observation and the analysis. L.J. and G.D. developed the flow tracking algorithm specific to the needs of this analysis. C.A.W. and P.T.Y. developed methods and software to integrate the flow tracking algorithm with these experiments and analysis. K.T.A., C.A.W. and G.D. developed algorithms for the F-actin turnover analysis. E.L.B. imaged myosin II localization. G.M.A., K.K. and E.L.B. collected the cell speed data and observed fixed cells under the different treatments; G.M.A. and C.A.W. analysed these data. M.A.T. performed experiments on detergent-extracted cytoskeletons and analysed the results. M.A.T., C.A.W. and J.A.T. wrote the paper. All authors discussed the results and commented on the manuscript.

Author Information Reprints and permissions information is available at www.nature.com/reprints. The authors declare no competing financial interests. Correspondence and requests for materials should be addressed to J.A.T. (theriot@stanford.edu).

METHODS

Keratocyte cultures and labelling. We cultured keratocytes from the scales of the Central American cichlid *Hypsophrys nicaraguensis* as described in ref. 25. Keratocytes from this species exhibit less cell-to-cell variability than those of goldfish (*Carassius auratus*) and black tetra (*Gymnocorymbus ternetzi*). We used cells that had been cultured for 18–36 h. Before microscopic observation, we treated the cells with 85% PBS containing 2.5 mM EGTA for approximately 5 min to break up sheets and obtain individually crawling cells. Only persistently polarized, fast-moving 'coherent' cells were analysed, as this subset of keratocytes maintains the most consistent shape and speed over time[26].

F-actin and myosin II were labelled in live keratocytes as described[25] by small-volume electroporation on the coverslip. For F-actin speckle visualization, we introduced Alexa Fluor 546 phalloidin (Molecular Probes) into the cells at low density. Cells were allowed to recover for approximately 15 min in complete medium. For myosin II visualization, we transfected keratocytes[26] with YFP-tagged *X. laevis* non-muscle myosin II regulatory light chain (a gift of A.F. Straight). Cells were allowed to recover for 18–24 h before treatment with EGTA.

Microscopy. We imaged cells at room temperature on a Nikon Diaphot-300 inverted microscope with a ×60 (numerical aperture 1.4) objective. We acquired phase contrast and epifluorescence images at 2-s (live cell experiments) or 10-s (extracted cytoskeleton experiments) time intervals with a 16-bit 512 pixel × 512 pixel cooled back-thinned charge-coupled device camera (Princeton Instruments). One pixel corresponded to 0.112 μm. All raw images displayed are single-image frames, except for Fig. 1f, which is a median projection from a 90-s movie (45 frames). Alexa Fluor 546 phalloidin and tetramethylrhodamine B isothiocyanate (TRITC)-phalloidin were excited with a narrow band excitation TRITC filter cube (Chroma Technology) to minimize light absorption by blebbistatin, thereby limiting photoinactivation[27] and phototoxicity[28].

Flow tracking. We measured movement of the actin network by using the adaptive multi-frame correlation algorithm with modifications described in ref. 25. We used a five-frame (10-s) temporal window, and a correlation template size adaptively adjusted between a minimum of 11 pixels × 11 pixels and a maximum of 21 pixels × 21 pixels. This algorithm assumes quasi-stationary network movement within the area of the template and over the duration of the temporal window. Motile keratocytes moved so rapidly that over the five-frame time window the requirement for stationarity could not be fulfilled. On the other hand, integration over five frames was necessary owing to the relatively low signal-to-noise ratio of the FSM images. Therefore, we performed the F-actin flow tracking in the cell frame of reference, in which the actin meshwork movement was approximately constant over a local neighbourhood in space and time. Speckle flow could then be tracked using the methods described in ref. 7. We removed isolated or grossly incoherent vectors from the raw flow data before resampling the flow field on a regular grid for visualization and further processing. We used the term 'perpendicular flow' to denote the component of flow perpendicular to the direction of cell movement.

Frames of reference. To define the transformations between the laboratory and cell reference frames, as well as to calculate cell speeds, we tracked whole-cell movement in the phase-contrast image sequences using the two-stage cross-correlation approach[8]. This track of cell movement approximated as rigid motion (translation and rotation) was then used to convert image sequences from the laboratory frame of reference (in which they were acquired) to the cell frame of reference for flow tracking; and then to convert flow measurements from the cell frame of reference to the laboratory frame of reference.

Region analysis. As different cells had slightly different sizes and shapes, comparison or averaging of F-actin velocity fields among different cells was difficult. Instead of using the velocity fields directly, we divided them into a set of five standard regions (illustrated in Supplementary Fig. 4b) in each cell and averaged the measurements within each region at each time point. This yielded a set of time series that could further be averaged over time to summarize a cell's steady-state actin-network movement pattern as a set of five velocity vectors. The five regions we manually defined in each cell were the following: rear left (when facing the direction of movement), front left, front centre, front right and rear right. Inward perpendicular flow for a cell was computed by taking the average of the perpendicular flow in the rear left region and the negated perpendicular flow in the rear right region.

Assembly and disassembly maps. To estimate the spatial pattern of net assembly and disassembly of the actin network, we used an algorithm based on steady-state flow field and intensity. We applied spatial smoothing to the flow field (resampled per pixel) and normalized the fluorescence image in each frame before computing the average over the length of the movie (30 s in Fig. 1e; 1 min in Fig. 2e). We then multiplied the average smoothed velocity field (v) by the average smoothed intensity (ρ) and calculated the divergence ($\nabla\cdot(\rho v)$) (similar to ref. 9) to obtain a steady-state assembly/disassembly map (see Supplementary Information for further details).

Pharmacological treatments. We performed pharmacological treatments during observation of the cells on the microscope, such that we were able to observe the changes that occurred as the drug took effect. The coverslip was mounted in a chamber for live-cell imaging with 1 ml medium above the coverslip. The medium was exchanged with one containing the desired drug or drug combination. For myosin II inhibition we used 100 μM (±)-blebbistatin (a gift of A. F. Straight) or 50 μM (−)-blebbistatin (the active enantiomer; Toronto Research Chemicals). We refer to the concentration of the active enantiomer in the main text. To promote myosin II activity, we used 25 μM calyculin A (Upstate Biotechnology). The F-actin stabilizing drug jasplakinolide (Molecular Probes) was used at 1 μM and the actin monomer sequestering drug latrunculin A (Molecular Probes) was used at 5 nM.

Fluorescence labelling of fixed cells. To examine the effect of blebbistatin or jasplakinolide on F-actin distribution, we fixed keratocytes with 4% formaldehyde for 15 min after a 15 min treatment with blebbistatin or jasplakinolide. We permeabilized the cells with 0.5% Triton X-100 in PBS for 10 min, blocked with 3% BSA in PBS with 0.1% Triton X-100 for 10 min, and labelled with 3.5 nM TRITC-phalloidin for 15 min before observation.

F-actin accumulation analysis. The F-actin accumulation analysis required additional steps, because fluorescence levels between cells could vary not only due to F-actin amount, but also due to fixation variations, phalloidin labelling efficiency and background fluorescence on the coverslip. We coarsely defined six regions in the phase-contrast image: front left, centre, right, and rear left, centre, right. To refine the regions, we manually segmented the cell interior by tracing its outline in the phase-contrast image. Note that this segmentation followed the overall contour of the cell without including any retraction fibres or 'tails'. The final regions were then defined as the intersection of the coarse regions and the cell interior.

We defined an additional background region in the phalloidin fluorescence image, and subtracted the median value of that region from the entire phalloidin fluorescence image, clamping to zero. We then computed the relative F-actin amount in each region as the ratio of the median phalloidin fluorescence in the region to the median phalloidin fluorescence in the front centre region. These ratios for the rear centre region are shown in Fig. 3g.

The rear 'tails' lie outside the cell interior traced as described above. We defined a minimum threshold for true fluorescence signal as the first centile value of (background-subtracted) fluorescence intensity inside the cell interior. Pixel locations that were outside the cell interior, inside the coarsely defined rear left and rear right regions and had (background-subtracted) values above the minimum threshold were classified as the rear 'tail' regions. The ratios of their median phalloidin fluorescence to median front-centre phalloidin fluorescence are shown in Fig. 3g.

Detergent-extracted cytoskeletons. To obtain Triton X-100-extracted keratocyte cytoskeletons, we cultured keratocytes on 22 mm × 40 mm coverslips. After treatment with EGTA, we attached the coverslips to microscope slides in orthogonal orientation to construct flow chambers containing the cells. Parafilm spacers were melted onto the slide at 80 °C before chamber assembly to form a 10-mm channel. We used silicone grease to seal the chamber and to construct an approximately 3 mm × 3 mm inlet port, which allowed fluid (including surfactant-containing buffers) to flow gently through the chamber by gravity, minimizing disruption of the specimen. We treated keratocytes essentially as in ref. 6 while observing them on the microscope. After quick rinses with Hank's balanced salt solution and cytoskeleton buffer[6] (50 mM imidazole, pH 7.4, 50 mM KCl, 0.5 mM $MgCl_2$, 0.1 mM EDTA, 1 mM EGTA), we exposed the cells to extraction buffer (cytoskeleton buffer containing 1% Triton X-100, 4% polyethylene glycol, relative molecular mass 40,000 and 0.2 μM TRITC-phalloidin) for approximately 30 s, then rinsed thoroughly with cytoskeleton buffer containing 0.2 μM TRITC-phalloidin and incubated for 5 min. Extraction buffer and all subsequent buffers added during the experiment contained an oxygen-scavenging system (2 mM DTT, 50 U ml^{-1} glucose oxidase (Sigma), 1,500 U ml^{-1} catalase (Sigma), 50 mM D-glucose) to minimize photobleaching.

To test for actin network disassembly, we perfused the chamber with assay buffer[20] (25 mM imidazole, pH 7.4, 25 mM KCl, 4 mM $MgCl_2$, 0.2 mM $CaCl_2$) and started time-lapse fluorescence imaging. Immediately after the indicated time points, we added assay buffer or assay buffer containing an ATP-regenerating system (1 mM ATP, 5 mM creatine phosphate (Sigma), 10 μg ml^{-1} creatine phosphokinase (Sigma)), 0.1 μM GST–villin (a gift of M. J. Footer) or both; the chamber was fully perfused by the new buffer before the next image acquisition occurred. To inhibit myosin II, we treated the cells with 50 μM blebbistatin before extraction for 30 min; in these experiments, every subsequently applied buffer contained 50 μM blebbistatin (or, in the control, the 0.1% dimethylsulphoxide vehicle).

For the experiments whose results are shown in Supplementary Fig. 6, imaging was performed through a ×40 (numerical aperture 0.85) objective using a 16-bit

1024 pixel × 1024 pixel cooled back-thinned charge-coupled device camera (Andor iXon+ DU-888).

Deformable substrates. We prepared gelatin-coated coverslips using a protocol derived from that of Doyle & Lee[29]. Heated (40 °C) 2.5% gelatin (200 μl) was added to each coverslip, then aspirated off, leaving a thin layer. Coverslips were cooled at 4 °C for 24 h. We then pipetted 0.5 ml media onto the gelatin and incubated it at 4 °C for 1 h. Afterwards we placed a fish scale and 27 μl media atop the gelatin on each coverslip and incubated at room temperature overnight. Before transferring a coverslip to the microscope for imaging, we incubated it briefly in a suspension of streptavidin-conjugated quantum dots (Molecular Probes). The quantum dots stuck non-specifically to the surface of the gelatin, acting as fiducial marks to allow observation of substrate deformation. (Note that because the streptavidin-conjugated quantum dots stuck non-specifically, some stuck to the dorsal surface of the cells as well.)

27. Sakamoto, T., Limouze, J., Combs, C. A., Straight, A. F. & Sellers, J. R. Blebbistatin, a myosin II inhibitor, is photoinactivated by blue light. *Biochemistry* **44,** 584–588 (2005).
28. Kolega, J. Phototoxicity and photoinactivation of blebbistatin in UV and visible light. *Biochem. Biophys. Res. Commun.* **320,** 1020–1025 (2004).
29. Doyle, A. D. & Lee, J. Cyclic changes in keratocyte speed and traction stress arise from Ca^{2+}-dependent regulation of cell adhesiveness. *J. Cell Sci.* **118,** 369–379 (2005).